Strain-hardening under uniaxial tension in a rejuvenated bulk metallic glass

W.H. Zhou[a,b], N.T. Panagiotopoulos[c], A.L. Greer[c,*], Y. Li[a,*]

[a]Shenyang National Laboratory for Materials Science, Institute of Metal Research, Chinese Academy of Sciences, Shenyang 110016, China

[b]School of Materials Science and Engineering, University of Science and Technology of China, Hefei, 230026, China

[c]Department of Materials Science & Metallurgy, University of Cambridge, Cambridge, CB3 0FS, UK

* Corresponding authors: alg13@cam.ac.uk; liyi@imr.ac.cn

Abstract

A rejuvenated Zr-based bulk metallic glass is tested in tension: it shows strain-hardening and reaches 0.9% plastic strain at failure. The initial rate of increase of flow stress with strain is 73 GPa, much higher than normal for polycrystalline metals and alloys. This hardening rate and its decay with increasing strain are compared with published data on a representative range of conventional and novel alloys. Taking the onset of necking as failure, and using Considère's analysis, we conclude that the metallic glass, however much rejuvenated, is limited to tensile plastic strains of approximately 1%, because of the rapid decay of hardening rate with strain. Rejuvenation of the metallic glass blocks early catastrophic failure in a predominant shear orientation. In comparison with as-cast samples, the fracture surface of the rejuvenated sample is more rugged and the characteristic vein pattern is denser. The effects of rejuvenation on abrasive-wear behavior are also examined.

Keywords: Metallic glass; Work-hardening; Ductility; Fracture; Tensile testing

For polycrystalline metals and alloys, the *ductility* (maximum plastic elongation in tension) underpins their importance in structural applications. Ductility follows from dislocation-mediated strain-hardening. In contrast, metallic glasses (MGs) deformed at room temperature (RT) show strain-softening [1], localizing flow in *shear bands* (Suppl. Mater. Fig. S1). While shear-banding permits substantial plastic deformation of MGs in constrained geometries (e.g. compression and bending), in uniaxial tension plastic-flow onset is followed almost immediately by catastrophic failure through primary shear that spans the specimen cross-section [2].

This macroscopically brittle behavior (negligible ductility) is the greatest impediment to wider exploitation of MGs in structural applications that otherwise would benefit from their high values of yield stress σ_y, elastic strain limit and resilience [3]. Comparison is commonly made between the plasticity of MGs in uniaxial compression (often misleadingly termed 'ductility') and the actual ductility of conventional engineering alloys that they might replace. The present work focuses on tension only.

With sufficient rejuvenation of a MG, strain-softening should be avoided [4]: plastic flow would be homogeneous (not localized into shear bands) even at RT (Fig. S1). Axial compression of notched bulk MG (BMG) rods at RT can rejuvenate the centre of the rods sufficiently to enable strain-hardening and suppress shear-banding in the rejuvenated material when subsequently tested [5]. This strain-hardening has mostly been characterized for specimens tested in uniaxial compression, but is also found in tension [5]. These preliminary results for tension are extended in the present work.

An alloy with nominal composition $Zr_{64.13}Cu_{15.75}Ni_{10.12}Al_{10}$ (at.%) was prepared by arc-melting mixtures of high-purity metals under a Ti-gettered high-purity argon atmosphere. BMG rods, diameter 5 mm and length 75 mm, were cast in copper molds. On each rod, a circumferential notch 1.5 mm deep and 0.45 mm wide was ground in a custom-built machine, followed by fine polishing [6,7]. Samples ~13 mm long with the notch at mid-length were cut from the rods. These samples were compressed

(Shimadzu AG-I machine) along the cylindrical axis until the notch width was reduced by ~45% [5,8]. The extracted centres of these rejuvenated samples were polished into dog-bone tensile specimens with a gauge of cross-section ~1.00×0.35 mm^2 and length ~2 mm (Fig. S2). Quasi-static uniaxial tensile tests (Instron-5848 micro-tester) used a 1×10^{-4} s^{-1} strain rate. Strain measurement based on digital image correlation (DIC) used random speckle patterns prepared by spraying black ink on a white background. Fracture surfaces were examined using scanning electron microscopy (Quanta 600 SEM, FEI), and their roughness was measured using confocal laser-scanning microscopy (CLSM). Differential scanning calorimetry (Q2000 DSC, TA Instruments) was at 20 K min^{-1} heating rate under flowing high-purity argon. Three-body abrasive-wear tests (Plint TE 66 microscale abrasion tester [9]) used a 25-mm-diameter-steel sphere, mounted on a rotating shaft, contacting the sample with a normal force of 0.05 N. With sliding speed 0.05 m s^{-1}, a slurry of 4-μm-diameter SiC particles in water (concentration 0.75 g cm^{-3}) was continuously applied. The wear volume was estimated from the diameter (up to 1.25 mm) of the crater in the specimen surface.

Figure 1 collects tensile (engineering stress)–(engineering strain) curves for an as-cast and two rejuvenated samples. The as-cast sample shows linear elasticity and catastrophic failure at an ultimate tensile stress (UTS, σ_U) of 1.68 GPa and final total strain ε_{tot} of 2.34%, of which the plastic strain at failure $\varepsilon_p \approx 0.02\%$. The data for Rej-2 are distinct (Table S1), but confirm the strain-hardening and tensile plasticity in Rej-1 [5]). Rej-2 has a σ_U (1.67 GPa) higher than for Rej-1, almost as high as the as-cast sample. Rej-2 has higher ε_p than Rej-1 (0.90% vs 0.68%). Figure 1 (inset) shows that, even in tension, plastic flow with strain-hardening continues after the onset of shear-banding indicated by serrations. This resembles the yielding of a Zr-based BMG rejuvenated by high-pressure torsion (HPT) [10].

Zr-based BMGs rejuvenated by cold-rolling [11] or by HPT [10] showed ε_p up to 0.27% and 1.05%, respectively, in subsequent tensile testing. This rejuvenation was attributed to shear-banding, and constitutes *shear-band engineering* [2] to improve plasticity. The present work (following [5]) focuses oppositely on shear-band

suppression.

We associate strain-hardening of rejuvenated MGs with structural relaxation [5,7], quantified using the heat of relaxation ΔH_{rel} (released on heating to the glass transition). Rejuvenation raises ΔH_{rel} from 0.50 kJ mol^{-1} for the as-cast sample to 1.25 kJ mol^{-1} (Figure S3). After tensile testing, ΔH_{rel} is reduced to 0.72 kJ mol^{-1} and 0.64 kJ mol^{-1} for Rej-1 and Rej-2 with $\varepsilon_p = 0.68\%$ and 0.90%, respectively. The lower value of ΔH_{rel} is associated with larger ε_p, confirming for tension the conclusion already reached for compression [5] that plastic flow induces structural relaxation.

Induced residual stresses have been used to increase the plasticity of MG specimens [2]. With the limited sample volume used for tensile testing in the present work, residual stresses should be too small to contribute significantly to the stored energy in the MG. Furthermore, rejuvenation of our samples increases their plasticity in both compression and tension, a result difficult to attribute to residual stresses. The ductility in the rejuvenated specimens is clearly associated with stored energy, distinct from effects of residual stress.

The strain-hardening and ductility of the Rej-2 sample permit comparison of its hardening-rate $\mathscr{H} = (d\sigma_T/d\varepsilon_T)$, profile as a function of ε_T in tension (σ_T, true stress; ε_T, true strain) with other metallic materials. Figure S4 surveys a wide range of conventional and novel polycrystalline metals and alloys [12–17]. The profile for Rej-2 is distinctive, with its initial hardening rate $\mathscr{H}_i$ of ~73 GPa (over an order of magnitude higher than for most conventional alloys, Table 1) decaying fast with increasing strain. The implications for failure in tension are considered in terms of the onset of necking, a more fundamental measure of mechanical performance than ε_{tot} [18]. Considère showed that a material is stable against necking while $(d\sigma_T/d\varepsilon_T) > \sigma_T$. Plotting both quantities as a function of strain, the onset of necking (at strain ε_n) is where the two curves intersect [18].

Such curves are compared for Rej-2, annealed commercial polycrystalline copper (ann-Cu) [18], and an ultrafine-grained dual-phase (ferrite-martensite) steel (UFG steel) [17] (Fig. 2). To facilitate comparison, σ_T and $\mathscr{H}$ are normalized with respect to the

ultimate tensile strength (i.e. the peak nominal stress). Annealing of copper reduces its σ_y and increases $\mathscr{H}$ at a given strain [18], and thus is analogous to rejuvenation of the BMG. Compared to annealed polycrystalline copper, the rejuvenated BMG has: much higher yield ratio (σ_y/σ_U), 0.78 vs 0.22, and normalized initial hardening rate ($\mathscr{H}_i/\sigma_U$), 44 vs 7; and a much lower plastic strain ε_p.

The UFG steel has a normalized $\mathscr{H}_i$ (~35) close to that of the BMG, yet shows a much higher ε_p. Comparing the three cases (Fig. 2) shows that the key factor determining ε_n (and therefore the likely ε_p) is the rate of decay of the hardening rate. For the BMG, failure occurs before the intersection of the curves. Comparison of the ε_p and ΔH_{rel} values for Rej-1 and Rej-2 shows that failure of Rej-1 occurs well before exhaustion of its capacity for structural relaxation and strain hardening. For Rej-1 and Rej-2, observed failure is not associated with the onset of necking, but rather with the shear-banding instability. Nevertheless, the near-vertical fall of ($d\sigma_T/d\varepsilon_T$) indicates that ε_p would be increased only marginally if shear-banding did not intervene: the BMG would fail (a sample in tension would start to neck) at a true strain of ~1%. If the BMG could be rejuvenated further, this would reduce the yield ratio and increase the initial hardening rate, but the decreasing ($d\sigma_T/d\varepsilon_T$) shows that the failure strain would not be significantly increased. This limit of $\varepsilon_p \approx 1\%$ matches the highest noted above for a BMG rejuvenated by HPT [10].

Whether considered in absolute value, or normalized with respect to σ_y (as in Ref. [5]), or to σ_U (as for Fig. 2), the initial hardening of the MG is remarkably fast (Table 1)—especially so, given that, unlike the UFG steel for example, the glass is a single phase with no microstructure (in any conventional sense). This efficiency of hardening limits the plastic strain achievable before the hardening capacity is exhausted. Hardening is by deformation-stimulated structural relaxation of the glass; if relaxation is hindered, hardening should be slower. Atomic mobility in MGs is dependent on the hydrostatic component of the applied stress, increasing when the component is tensile and vice versa. This dependence explains the opposite effects of tensile and compressive loading in notched regions of BMG cylinders [7,8]. In the present case

(without constraints of notch geometry), the rejuvenated BMG hardens (relaxes) when tested in tension and compression, but as expected the hardening rate is lower in compression. Importantly, the lowered rate also decays more slowly with strain (Fig. S4). If that lowered rate were achieved in tension, the failure strain would be just under 1.5%. (In actual compression of the rejuvenated BMG, strains exceeding 20% are achieved without failure [5].) Given that the profile of $(d\sigma_T/d\varepsilon_T)$ vs ε_T is favorably broadened when atomic mobility is reduced, we suggest lowering the test temperature to achieve greater plastic strains in tension.

For an as-cast sample (Fig. 3a,b), the fracture surface is largely planar, a single shear band dominates the fracture. The angle between the fracture plane and the tensile axis, is 55° in the across-width direction and 53° in the through-thickness direction, consistent with previous observations [19]. In contrast, for rejuvenated samples (Fig. 3d,e), the surface is rugged, final fracture involves multiple shear bands, and shearing is only in the through-thickness direction at 53° to the tensile axis. On stress-strain curves (inset in Fig. 1), serrations appear for $\varepsilon_p > 0.62\%$, indicating suppression of shear-banding up to that point.

The fracture surfaces show the vein patterns characteristic of MGs. The pattern is sparse for the as-cast sample, (Fig. 3c), but dense and uniform for rejuvenated samples (Fig. 3f). Fracture-surface morphologies (Fig. 4a,b) and height profiles (Fig. 4c,d) are quantified using laser-scanning confocal microscopy. For the as-cast sample, as noted, the fracture surface is flat: profiles along orthogonal directions in the fracture plane show height variation of <3 μm. For the rejuvenated sample, the rugged fracture surface shows peaks and valleys, and the height variation reaches a maximum of 18 μm.

Rejuvenation of Zr-based BMGs by HPT similarly led to rugged fracture surfaces after tensile testing [10]. Finer-scale roughness was not reported, but is examined in the present work. Height profiles for two locations (red boxes on Fig. 4a,b) are examined in close-up (Fig. S5). The average roughness R_a for as-cast and Rej-2 samples along through-thickness and across-width directions is always approximately 0.04 μm (Fig. S5c,f).

For as-cast BMGs in tension, the end of the elastic regime occurs at a σ_y high enough to drive catastrophic shear failure across the sample, from a single initiation point. The present work confirms that rejuvenation blocks this catastrophic mode. Plastic flow starts at lower stress and is distributed such that there no single initiation point; the fracture is more complex and the surface is rugged. The final fracture in each case involves liquid-like flow in a thin layer [2]. In as-cast samples there is a significant shear offset before the vein pattern develops as the two ends of the sample finally part (Fig. 3c and Fig 4a). The rugged geometry in rejuvenated samples limits the shear offset and a dense vein pattern predominates (Fig. 3f and Fig 4b). This pattern has its origin in the Saffman-Taylor instability in the liquid-like layer between material separating in the direction normal to the layer (i.e. in the manner of a Type-I crack).

Xi et al. showed that the scale w (width of dimples, or spacing of ridges) of the patterns on the fracture surface of MGs is a guide to the plastic process zone size [20]. Higher w correlates with higher normalized toughness. In the present case, the as-cast sample shows a characteristic dimple size with $w \leq 50$ μm. The rejuvenated sample shows a dimple size with $w \geq 50$ μm. These values are as suggested in ref. [20] for Zr-based MGs, and are at the upper limit of the measured range of w. Our samples appear to be as tough as expected for Zr-based BMGs, without rejuvenation having any significant effect.

Strain-hardening is of interest for the wear resistance of MGs. For both polycrystalline pure metals and as-cast MGs, the abrasive-wear resistance W_R (the inverse of the wear coefficient K) increases linearly with hardness H in the steady state established after a running-in period [21]. For a given value of H, W_R is (4–5)× higher for the pure metals. This is attributed to strain-hardening: effectively, wear is measured for a surface that is harder than the original sample [21]. On a vertical section of a rejuvenated BMG (similar to that shown in Fig. 2c in Ref. [8]), W_R was measured at two locations far from the notch (As-cast) and one location near the notch root (Rej) under microscale-abrasion conditions as used earlier [21,22]. The wear

behavior of the two 'As-cast' regions broadly matches published data on an as-cast BMG of similar composition (Fig. S6). The 'Rej' region of the sample is unfortunately so small that its wear behavior can be characterized only in the running-in period before the steady state. The W_R of the 'Rej' region would be about 20% less if it scaled with the local hardness, but it is within experimental uncertainty identical to that of the 'As-cast' regions. This is consistent with strain-hardening in the wear test restoring the worn surface to a condition similar to the original glass.

The present work extends to 0.9% the maximum tensile plastic strain of a monolithic BMG rejuvenated by homogeneous plastic flow. The reduction in heat of relaxation seen earlier is confirmed to continue as the plastic strain increases. This reduction corresponds to structural relaxation, leading to desirable strain-hardening. The limits to achievable plastic strain are evaluated using the Considère analysis of the onset of necking. For the rejuvenated BMG in the present work, fracture occurs before the predicted onset of necking. The analysis shows, however, that even if much greater rejuvenation could be achieved, the plastic strain would be inevitably limited to ~1%. Comparison with a wide range of conventional and novel metallic materials shows that this limit comes from the rapid decay of the hardening rate. Nevertheless, rejuvenation is effective at blocking catastrophic single-shear-plane failure in tension.

Acknowledgements

We acknowledge support from the European Research Council: for A.L.G. and N.T.P. under the Advanced Grant "ExtendGlass – Extending the range of the glassy state: Exploring structure and property limits in metallic glasses" (grant ERC-2015-AdG-695487). Y.L. and W.H.Z acknowledge financial support from the Shenyang National Laboratory for Materials Science.

References

[1] F. Spaepen, Acta Metall. 25 (1977) 407–415.

[2] A.L. Greer, Y.Q. Cheng, E. Ma, Mater. Sci. Eng. R. 74 (2013) 71–132.

[3] M.F. Ashby, A.L. Greer, Scr. Mater. 54 (2006) 321–326.

[4] Y.H. Sun, A. Concustell, A.L. Greer, Nat. Rev. Mater. 1 (2016) 16039.

[5] J. Pan, Y.P. Ivanov, W.H. Zhou, Y. Li, A.L. Greer, Nature 578 (2020) 559–562.

[6] J. Pan, Y.X. Wang, Y. Li, Acta Mater. 136 (2017) 126–133.

[7] Z.T. Wang, J. Pan, Y. Li, C.A. Schuh, Phys. Rev. Lett. 111 (2013) 135504.

[8] J. Pan, Y.X. Wang, Q. Guo, D. Zhang, A.L. Greer, Y. Li, Nature Commun. 9 (2018) 560.

[9] R.I. Trezona, D.N. Allsopp, I.M. Hutchings, Wear 225–229 (1999) 205–214.

[10] S.H. Joo, D.H. Pi, A.D.H. Setyawan, H. Kato, M. Janecek, Y.C. Kim, S. Lee, H.S. Kim, Sci. Rep. 5 (2015) 9660.

[11] Q.P. Cao, J.W. Liu, K.J. Yang, F. Xu, Z.Q. Yao, A. Minkow, H.J. Fecht, J. Ivanisenko, L.Y. Chen, X.D. Wang, S.X. Qu, J.Z. Jiang, Acta Mater. 58 (2010) 1276–1292.

[12] Y. Wu, Y.H. Xiao, G.L. Chen, C.T. Liu, Z.P. Lu, Adv. Mater. 22 (2010) 2770–2773.

[13] Q.S. Pan, H.F. Zhou, Q.H. Lu, H.J. Gao, L. Lu, Nature 551 (2017) 214–217.

[14] C.L. Yang, Z.J. Zhang, T. Cai, P. Zhang, Z.F. Zhang, Sci. Rep. 5 (2015) 15532.

[15] J.H. Gao, Y.H. Huang, D.K. Guan, A.J. Knowles, L. Ma, D. Dye, W.M. Rainforth, Acta Mater. 152 (2018) 301–314.

[16] T.S. Byun, N. Hashimoto, K. Farrell, Acta Mater. 52 (2004) 3889–3899.

[17] M. Calcagnotto, Y. Adachi, D. Ponge, D. Raabe, Acta Mater. 59 (2011) 658–670.

[18] T.W. Clyne, J.E. Campbell, *Testing of the Plastic Deformation of Metals*, Cambridge University Press, Cambridge, 2021.

[19] Z.F. Zhang, G. He, J. Eckert, L. Schultz, Phys. Rev. Lett. 91 (2003) 045505.

[20] X.K. Xi, D.Q. Zhao, M.X. Pan, W.H. Wang, Y. Wu, J.J. Lewandowski, Phys. Rev. Lett. 94 (2005) 125510.

[21] A.L. Greer, K.L. Rutherford, I.M. Hutchings, Inter. Mater. Rev. 47 (2002) 87–112.

[22] A.L. Greer, W.N. Myung, Mater. Res. Soc. Symp. Proc. 644 (2001) L10.4.1–L10.4.12.

TABLES

Table 1. The initial hardening rate $\mathscr{H}_i = (d\sigma_T/d\varepsilon_T)_i$ at the onset of plastic flow for a variety of conventional and novel polycrystalline alloys tested in tension, and for rejuvenated BMG samples tested in tension or compression. The materials can be compared in terms of the absolute values of $\mathscr{H}_i$, or the values $\mathscr{H}_i/\sigma_y$ and $\mathscr{H}_i/\sigma_U$ normalized with respect to the yield stress and ultimate tensile stress respectively. All values are in GPa.

Alloy	$\mathscr{H}_i$ (GPa)	σ_y	$\mathscr{H}_i/\sigma_y$	σ_U	$\mathscr{H}_i/\sigma_U$
Rejuvenated BMG in tension†	73.0	1.30	56.2	1.67	43.7
Rejuvenated BMG in tension*	67.0	1.27	52.8	1.61	41.6
Rej. BMG in compression‡	59.0	1.32	44.7	1.70	34.7
BMG composite [12]	42.0	1.30	32.3	1.65	25.5
CG-Cu [13]	2.7	0.08	33.8	0.23	11.7
UFG-Cu [13]	9.0	0.37	24.3	0.38	23.6
NT-Cu [13]	12.6	0.33	38.2	0.39	32.3
Ni-0.5Si alloy annealed [14]	4.6	0.09	51.1	0.36	12.8
Ti-7Mo-3Cr annealed [15]	4.0	0.70	5.7	0.91	4.4
316 steel annealed [16]	2.1	0.30	7.0	0.60	3.5
CG ferrite/martensite steel [17]	34.0	0.45	75.6	0.87	39.1
UFG ferrite/martensite steel [17]	36.0	0.53	67.9	1.04	34.6

†The Rej-2 sample of $Zr_{64.13}Cu_{15.75}Ni_{10.12}Al_{10}$ BMG in the present work.
*The Rej-1 sample from Ref. [5].
‡Data on a different sample of the same BMG, from Ref. [5].

Figures

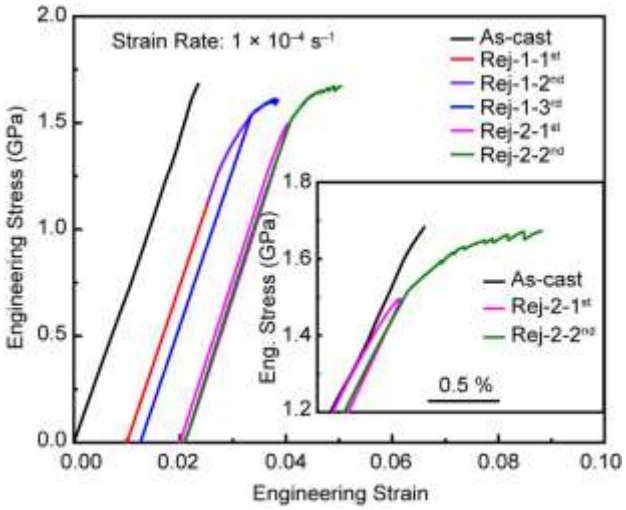

Fig. 1. Tensile (engineering stress)–(engineering strain) curves for an as-cast and two rejuvenated samples of the $Zr_{64.13}Cu_{15.75}Ni_{10.12}Al_{10}$ BMG. The data on 'As-cast' and 'Rej-1' were reported in Ref. [5]. The testing of Rej-1 included two unloading segments; Rej-2 was tested with one unloading segment. The curves for Rej-1 and Rej-2 are offset by 1% and 2% for clarity. The inset shows a close-up of the onset of yielding in As-cast and Rej-2.

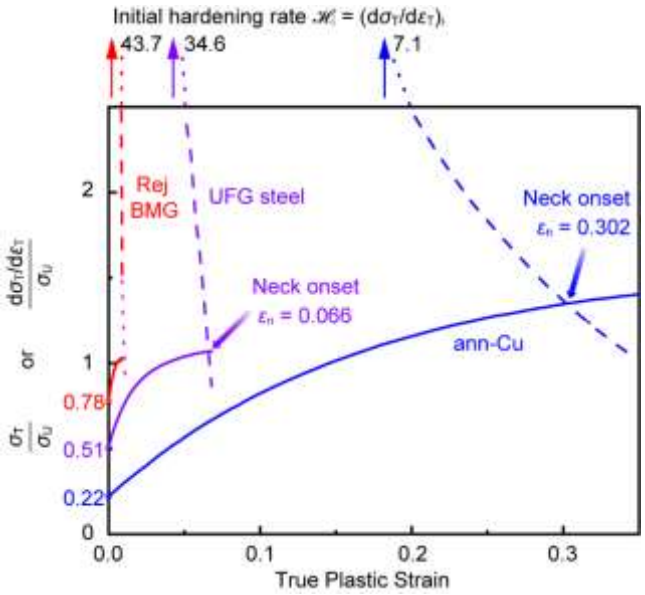

Fig. 2. Normalized values of flow stress σ_T (solid lines) and hardening rate $d\sigma_T/d\varepsilon_T$ (dashed lines) as a function of true plastic strain in tension for: Rej-2 (Rej BMG, red); annealed commercial polycrystalline copper (ann-Cu, blue), and an ultrafine-grained dual-phase steel (UFG steel, purple). Necking is expected for strains beyond the intersection of the solid and dashed lines. The Rej BMG fails before the intersection is reached; the virtual strain for the onset of necking is estimated by extrapolation of $d\sigma_T/d\varepsilon_T$ (pink dotted line).

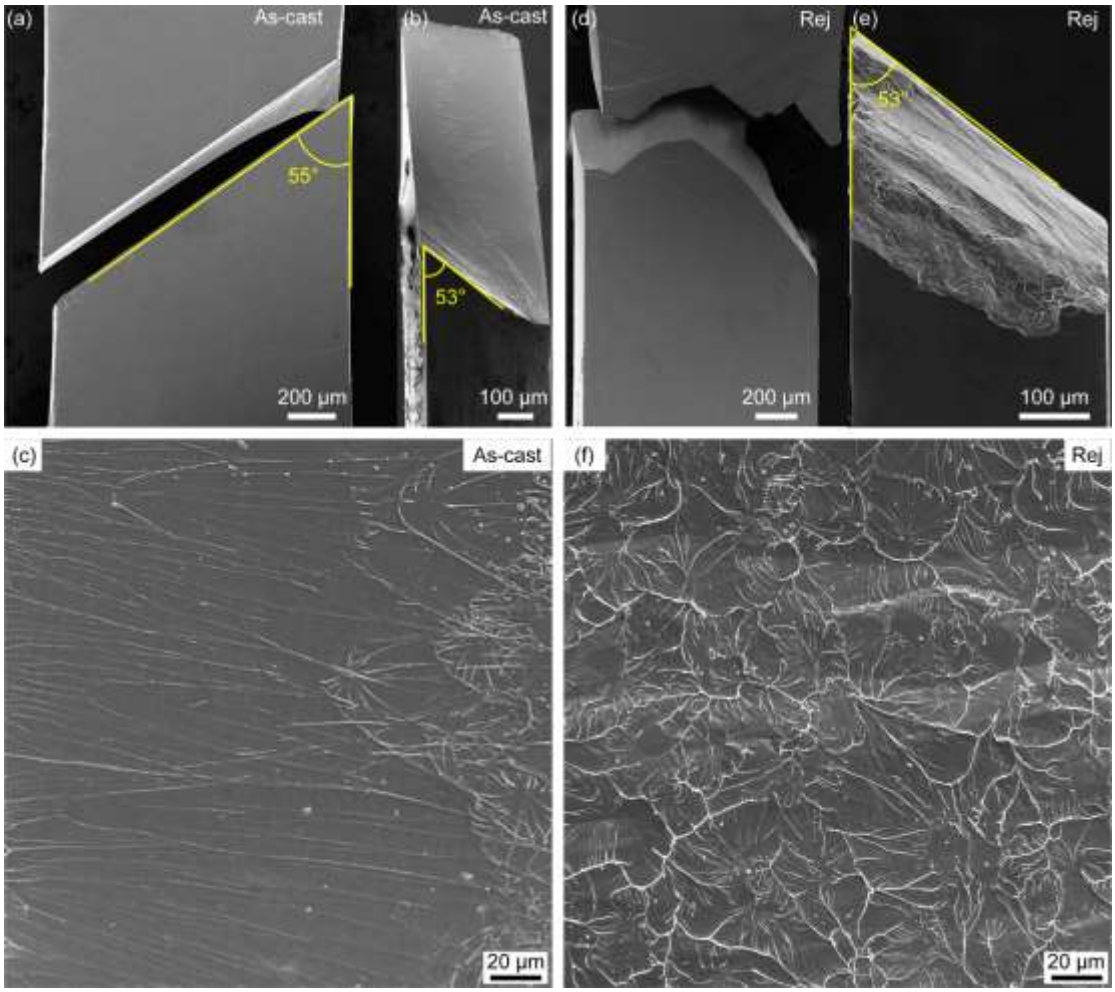

Fig. 3. SEM micrographs of the tensile fracture of as-cast and rejuvenated samples of the Zr-based BMG. General views of shear fracture across the width and thickness of: (**a,b**) the as-cast sample; (**d,e**) the rejuvenated sample (Rej-2). The fracture surfaces (**c**, as-cast; **f**, rejuvenated) show vein patterns.

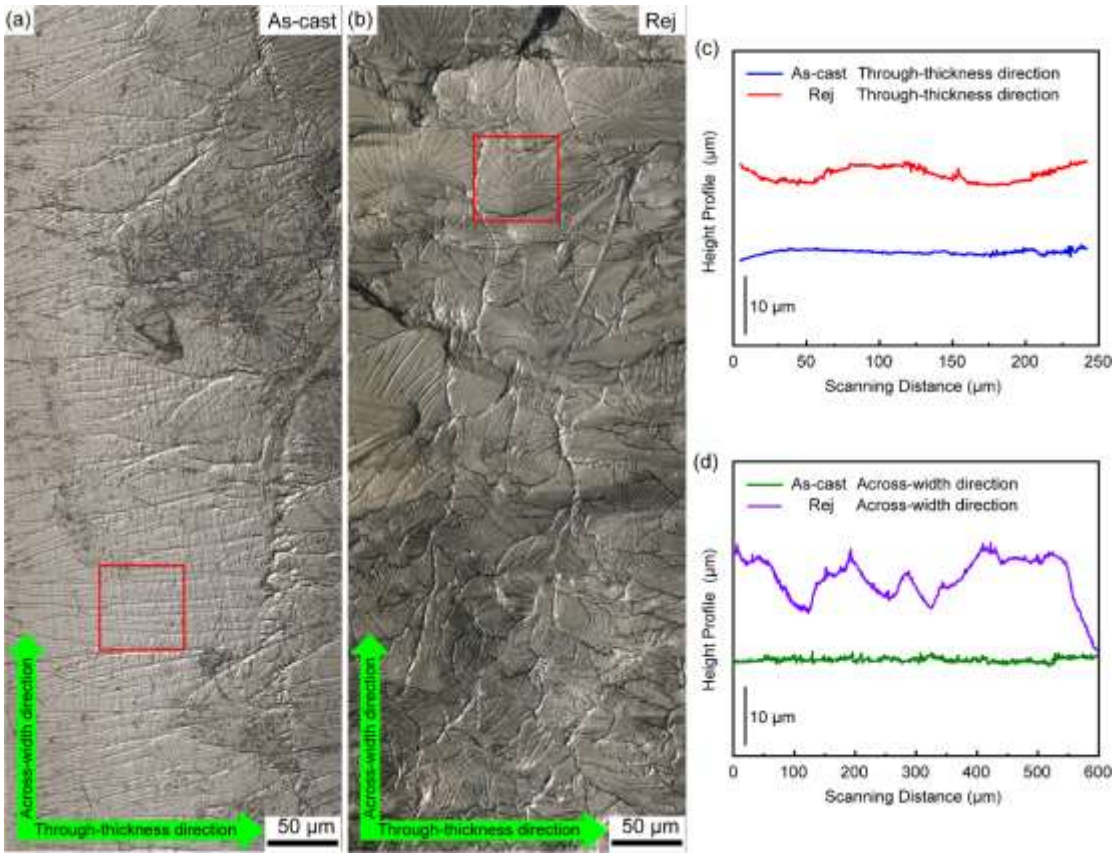

Fig. 4. Confocal microscopy of the fracture-surface morphologies for the Zr-based BMG: (**a**) as-cast; (**b**) rejuvenated. The red frames show the locations used for characterization of roughness (Fig. S.5). Line profiles of height variation in the (**c**) through-thickness, and (**d**) across-width directions, are compared for as-cast and rejuvenated samples.

Supplementary Information

Strain-hardening under uniaxial tension in a rejuvenated bulk metallic glass

W.H. Zhou, N.T. Panagiotopoulos, A.L. Greer, Y. Li

Table S1. Young modulus (E), initial yield stress (σ_y), plastic strain at the onset of serrations (ε_s), plastic strain at failure (ε_p), ultimate tensile stress (σ_U), exothermic heat of relaxation ΔH_{rel} and local average roughness (R_a) of the fracture surface in the through-thickness direction for the samples after tensile testing. Some of the values for the As-cast and Rej-1 samples were previously given in Ref. [5].

Sample	E	σ_y	ε_s	ε_p	σ_U	ΔH_{rel} (kJ mol^{-1})		R_a
	(GPa)	(GPa)	(%)	(%)	(GPa)	Undef	Def	(μm)
As-cast	73±5	1.66	0	<0.02	1.68	0.50		0.037±0.06
Rej-1	74±5	1.27	0.57	0.68	1.61	1.25	0.72	—
Rej-2	77±5	1.30	0.62	0.90	1.67	1.25	0.64	0.035±0.06

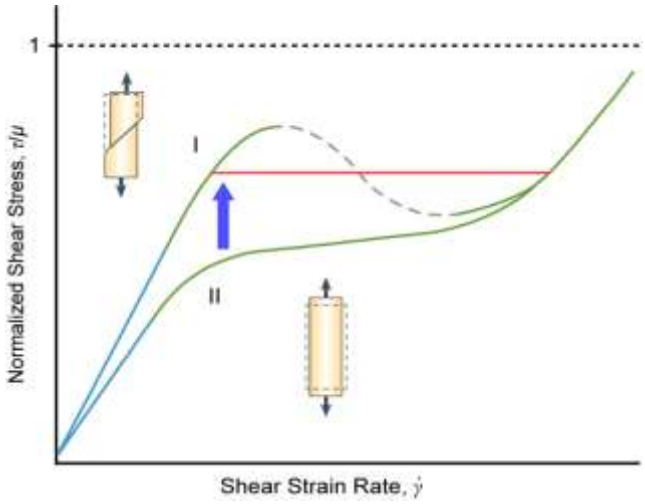

Fig. S1. Plastic deformation of a metallic glass (MG). Sketches of applied shear stress τ, normalized by the shear modulus μ, as a function of shear strain rate $\dot{\gamma}$. Curve I shows the usual progression for an as-cast glass from linear Newtonian flow (blue line) to non-Newtonian (green line) with an unstable regime (dashed line). In the shear-banding instability (red line, and inset top left), found in MGs tested at RT, two values of $\dot{\gamma}$ co-exist at the same τ. It is postulated in Ref. [4] that with sufficient rejuvenation of the initial glass this instability would be avoided (Curve II) and flow would be homogeneous (inset bottom right). The present work shows (Fig. 2) that the stable flow made possible by rejuvenation of the MG is very limited in extent. When the rejuvenated MG is deformed, its structure undergoes rapid relaxation, thus reverting (as schematically shown by the broad arrow) towards the as-cast state (i.e. from Curve II towards Curve I). This rapid reversion and its consequences in limiting ductility were not foreseen in Ref. [4]. (Adapted with permission from Ref. [4].)

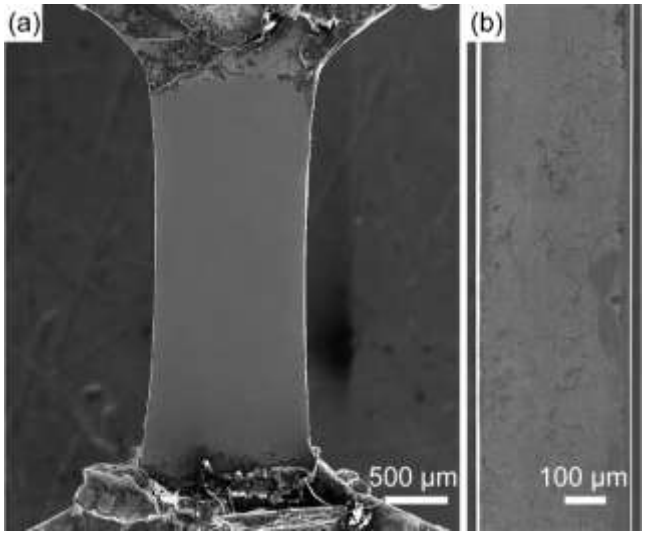

Fig. S2. The gauge length of sample Rej-2 of rejuvenated $Zr_{64.13}Cu_{15.75}Ni_{10.12}Al_{10}$ BMG. Scanning electron micrographs of (**a**) the main face, (**b**) side view.

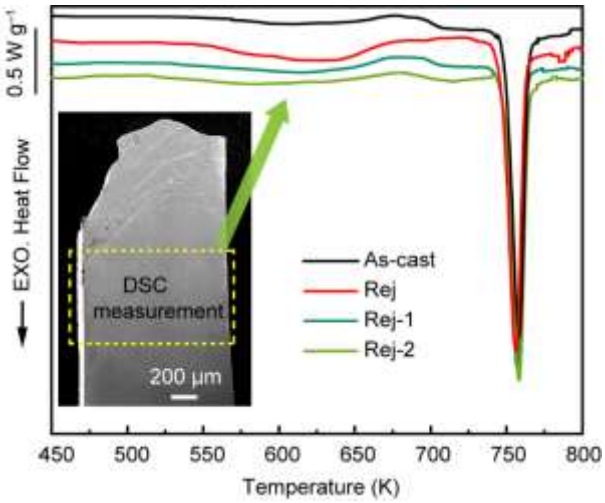

Fig. S3. Differential scanning calorimetry of $Zr_{64.13}Cu_{15.75}Ni_{10.12}Al_{10}$ MG samples heated at 20 K min^{-1}: as-cast (black), rejuvenated (red), and rejuvenated and then deformed to fracture in uniaxial tension (Rej-1 blue and Rej-2 green). The dashed box in the inset shows the portion of the fractured Rej-2 sample used for the DSC measurement of the rejuvenated and deformed MG, and the arrow indicates the associated DSC trace. Details of the samples are in Table S1.

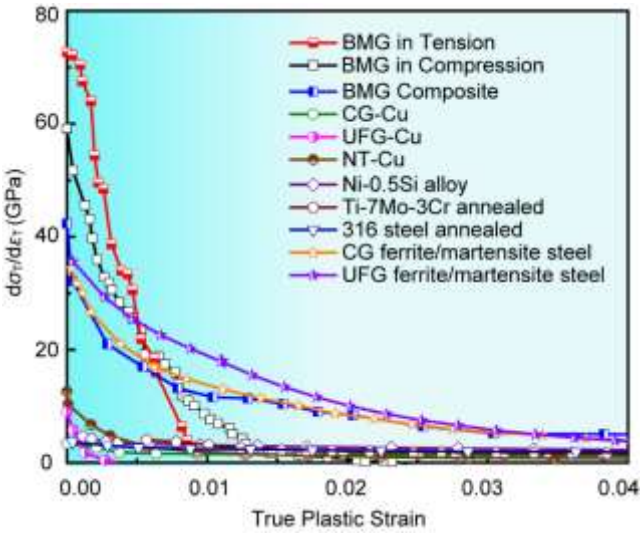

Fig. S4. The hardening rate $\mathscr{H} = (d\sigma_T/d\varepsilon_T)$ as a function of true plastic strain during flow of a variety of alloys. Data are shown for the present rejuvenated $Zr_{64.13}Cu_{15.75}Ni_{10.12}Al_{10}$ BMG tested in tension and compression. All the other data, for conventional and novel polycrystalline alloys, are for samples tested in tension. Details of the materials and the sources of data are given in Table 1.

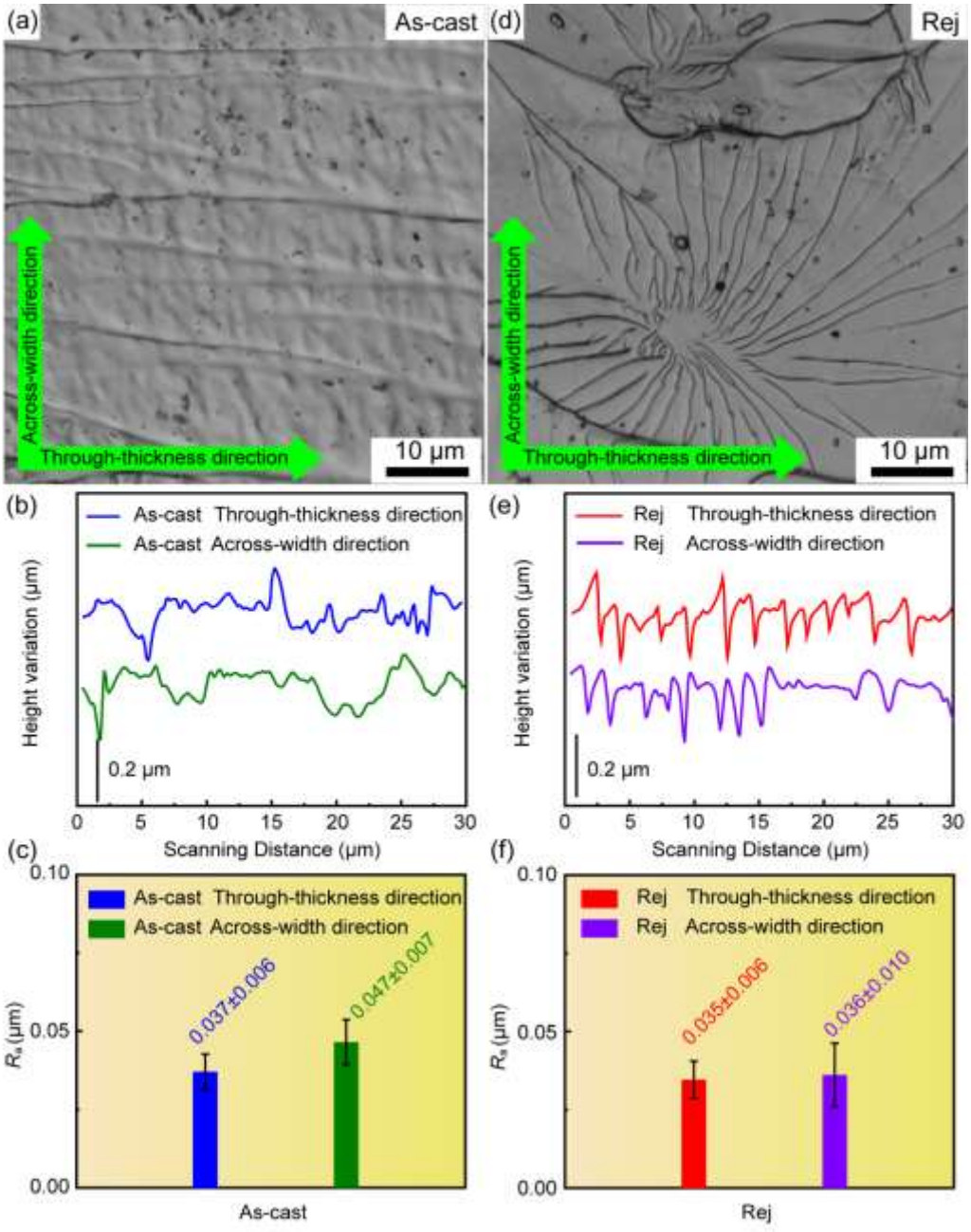

Fig. S5. Confocal-microscopy characterization of fracture surfaces for (**a–c**) as-cast, and (**d–f**) rejuvenated (Rej-2) MG samples. (**a,d**) close-ups of the boxed areas in Fig. 4a,b. (**b,e**) line profiles of height variation in the through-thickness and across-width directions in these selected areas. (**c,f**) the corresponding average surface roughnesses R_a.

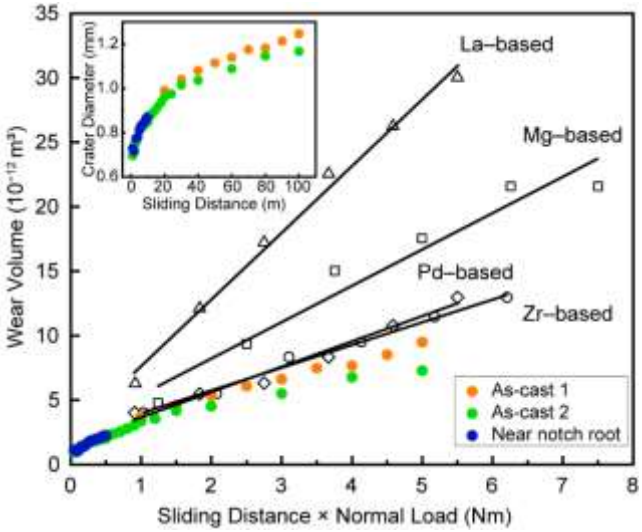

Fig. S6. Three-body abrasive wear of BMGs. In these microscale abrasion tests [9], in all cases, the volume of wear craters increases linearly with sliding distance according to the Archard wear equation [21]. The open black data points show published data for four BMGs ($La_{60}Al_{20}Ni_{10}Co_5Cu_5$, $Mg_{65}Ni_{20}Nd_{15}$, $Pd_{40}Ni_{10}Cu_{30}P_{20}$, and $Zr_{55}Al_{10}Ni_5Cu_{30}$) [21,22]. Data for the $Zr_{64.13}Cu_{15.75}Ni_{10.12}Al_{10}$ BMG in the present work lie close to the published data for the Zr-based BMG. Importantly, the data for the rejuvenated (near-notch) portion of the present glass (blue dots) superpose on the data from regions of the sample far from the notch, representing the as-cast state. This superposition is particularly clear in the inset, showing the raw data of crater diameter vs sliding distance. The rejuvenation reduces the hardness of the BMG by ~20%, and according to the Archard wear equation this would lead to a corresponding increase in the crater volume. That rejuvenation does not decrease the wear resistance is interpreted in terms of strain hardening (see main text).